were operated to investigate their effects on the lunar surface.

Types of Lunar Soil Erosion

Terrestrial tests have demonstrated that the vertical and horizontal shear forces exerted by rocket gases impinging on a horizontal soil surface could cause lunar surface erosion or cratering by three basic processes:

(1) Viscous erosion. Entrainment of soil particles as the exhaust gases flow over the surface (refs. 4–14 and 4–15, theoretical studies; ref. 4–16, an experimental study).

(2) Diffused gas erosion. Movement of soil caused by the outward and upward flow of gas through the pores of the soil (ref. 4–17). An eruption of the soil could occur if an engine is rapidly shut down.

(3) Bearing load cratering (also called explosive cratering). Rapid cratering caused when the exhaust gas pressure on a surface exceeds the bearing capacity of the surface (ref. 4–18). With the full expansion of Surveyor exhaust plumes in the lunar environment, this type of erosion was not likely to occur.

Vernier-Engine Firings

Surveyor III provided the first indication of the erosion effects of rocket gases on the lunar surface. The firing of the vernier engines during the Surveyor V mission was intended primarily to determine the diffused-gas eruption effects resulting from rapid engine shutdown. Surveyor VI engines were fired at a higher thrust level, and for a longer period of time, to increase the viscous erosion effects.

Observations

SURVEYOR III. The vernier engines of Surveyor III continued to fire during the first two touchdowns. The site of the second touchdown was visible to the camera from the final landed position, approximately 11 meters away. As seen in figure 4–8, not only are the imprints of the three footpads visible, but also a light streak of soil can be seen with adjacent dark soil; both light and dark soil are attributed to the firing of vernier engine 3. However, other than the indication that the vernier engines probably caused soil erosion, little additional information could be obtained.

SURVEYOR V. On September 13, 1967, 53 hours after landing, the Surveyor V vernier engines were fired at low thrust for 0.55 second. Engines 1 and 3 were fired at thrusts of 120 N; engine 2 was fired at 76 N. Study of Surveyor television pictures has shown that even though the spacecraft was resting on the inner slope of a small crater at an angle of about 20° (fig. 4–16), the firing caused no downslope motion of the spaceframe. The firing, however, did move the sensor head of the alpha-scattering instrument, which was resting on the lunar surface. During the firing, the sensor head rotated 15°, and its center of gravity moved 10 cm in a direction 45° from the direction of maximum slope. The lunar weight of the sensor head was 4.4 N. Two types of soil erosion occurred:

(1) Viscous erosion. A thin layer of soil was removed from beneath and adjacent to the vernier engines (fig. 4–17). Erosion of soil during the firing extended to distances at least up to 1.9 meters from the engines. As shown in the controlled [3] mosaics (fig. 4–18), the soil layer near vernier engine 3 and adjacent to the sensor head was substantially disturbed by the firing. Some of the soil and rock fragments moved by the firing are identified on these annotated mosaics. The largest fragment known to have been moved is 4.4 cm in diameter. Television pictures indicate that, at least in some places, soil was disturbed by viscous erosion to depths probably greater than 1 cm for distances up to 60 cm from engine 3. As shown in figure 4–18, soil at *E*, beside rock *a*, was eroded to a depth of about 1 cm. The trail (fig. 4–18(a)) left by rock *H* as it rolled downslope is no longer visible (fig. 4–18(b)). Figure 4–19 shows the relative distance that fragments of different sizes can be moved by gases striking the lunar surface with surface pressures equivalent to those of vernier engine 3 (ref. 4–3). This figure shows that fragments up to 4 or 5

[3] The controlled mosaics are composed of narrow-angle television frames mounted on a spherical surface; the center and orientation of each frame are correct relative to all other frames.

339–462 O—69——11

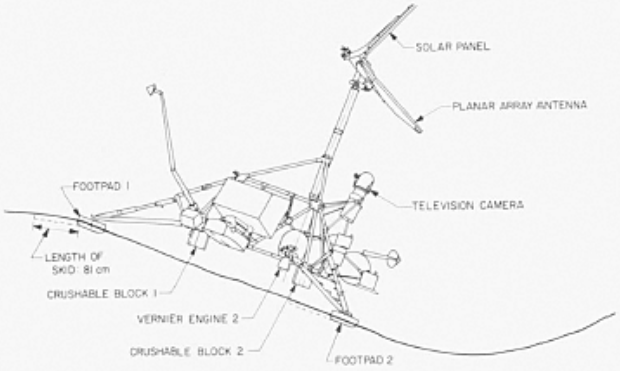

FIGURE 4–16.—Profile of Surveyor V and the crater in which it landed.

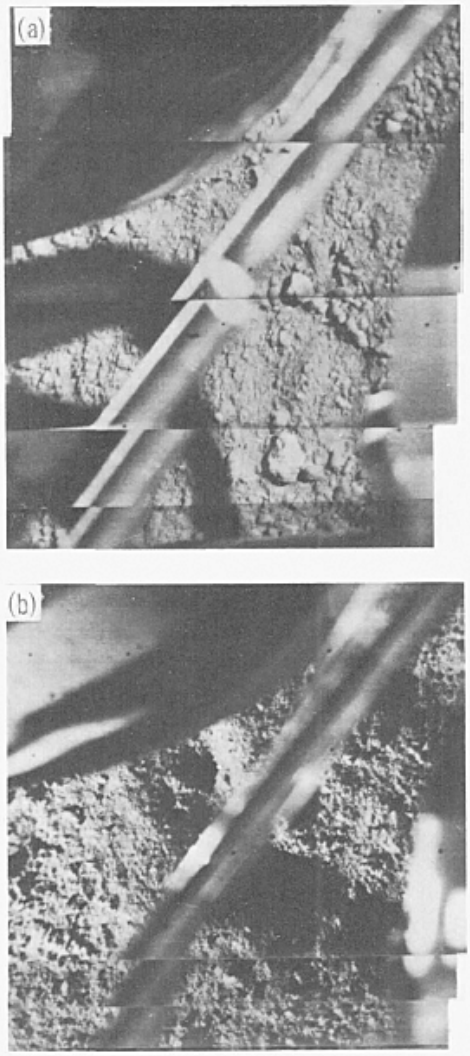

FIGURE 4–17.—Lunar surface beneath Surveyor VI vernier engine 3, as seen through an auxiliary mirror. (a) Prefiring picture. (b) Postfiring picture, showing the shallow crater caused by diffused gas eruption at engine shutdown.

cm in diameter were moved at distances up to approximately 20 cm; whereas, at distances of 200 cm, only fragments up to 0.4 cm in diameter were moved.

(2) Diffused gas erosion. Exhaust gases, which had diffused into the soil during the firing, caused the soil to erupt at engine shutdown and form a shallow, crescent-shaped crater (fig. 4–17(b)). The crater is 20 cm in diameter and 0.8 to 1.3 cm deep; the height of the vernier engine above the surface was 39 cm, and the maximum static pressure of the exhaust gases on the surface directly below the engine was 0.29 N/cm^2. Prefiring and postfiring pictures of the lunar surface below engine 3 are shown in figure 4–17.

SURVEYOR VI. On November 17, 1967, 177 hours after landing, the Surveyor VI vernier engines were fired for 2.5 seconds in order to lift the spacecraft from the lunar surface and to move it a short distance from the original landing site. This maneuver subjected the lunar surface to greater erosional forces from the vernier-engine exhaust gases than that exerted during the Surveyor V static firing. To achieve horizontal motion during the hop, the spacecraft's flight control system had been preset by Earth command such that the spacecraft acquired a tilt of 7° immediately following liftoff (fig. 4–20). This 7° tilt of the vernier engines caused soil eroded by the exhaust gases to be preferentially ejected to the east, away from the tilt direction (fig. 4–21).

Figure 4–22 is a mosaic of computer-enhanced pictures of the first landing site identifying the double imprints formed by the footpads and the single imprints formed by the crushable blocks during the original landing; the locations of the vernier engines before liftoff for the hop are also shown. On figure 4–22, the major areas of erosion caused by vernier-engine exhaust gases are identified with capital letters. Areas *A–E* represent erosion principally attributed to vernier engine 2, areas *G–I* to engine 3, and areas *K–N* to engine 1 (ref. 4–4). Enlargements of the main erosion areas for each engine are shown in figures 4–23 through 4–25.

Some of the more pronounced erosion features, formed by the firing and visible in

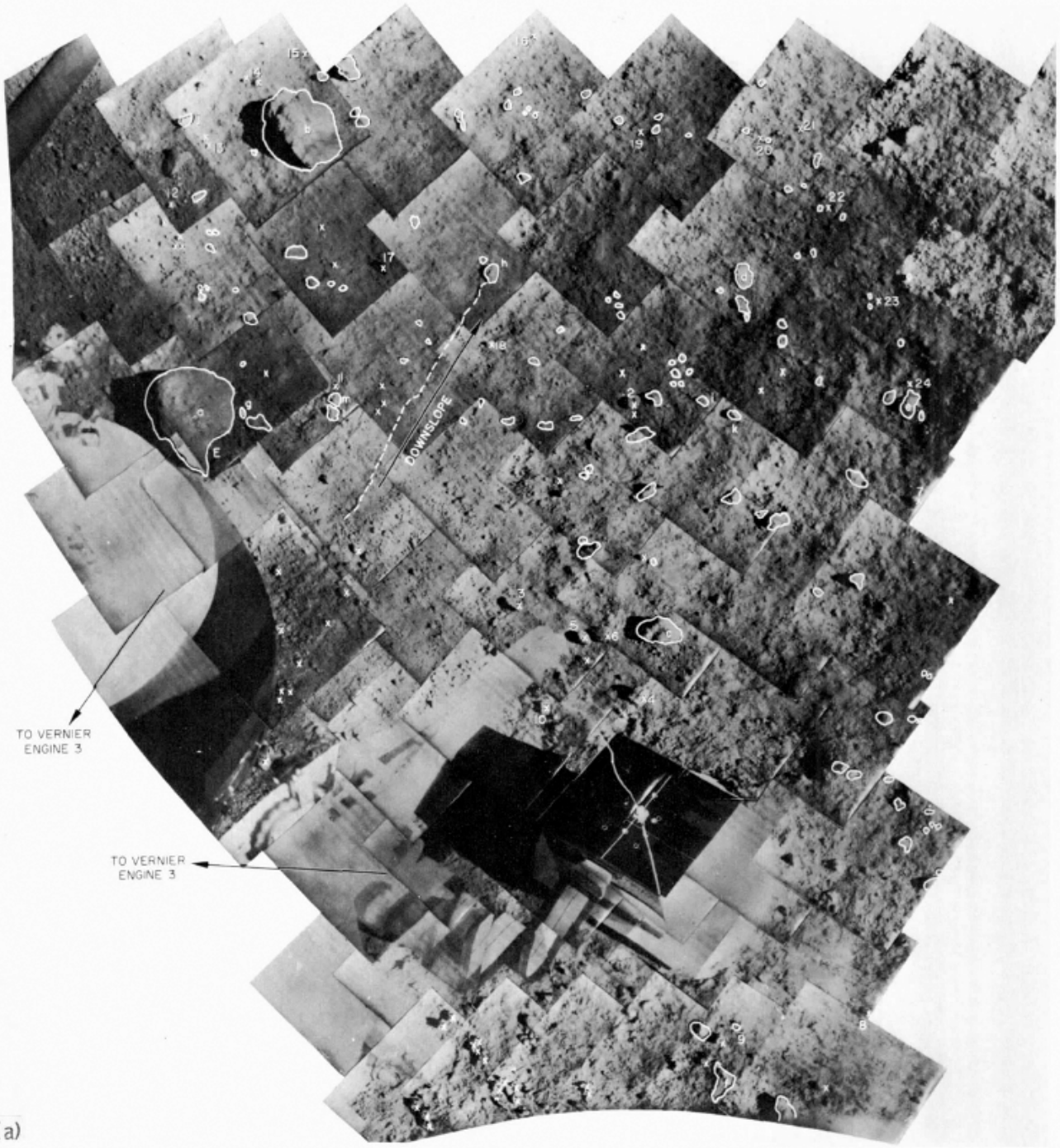

(a)

FIGURE 4–18.—(a) Prefiring, annotated mosaic of alpha-scattering-instrument area. Rock and soil fragments not moved by the firing are outlined; fragments shown by postfiring pictures to have been moved by the firing are marked with an X (Sept. 10, 1967). (b) Postfiring, annotated mosaic of alpha-scattering-instrument area. Fragments not moved by the firing are outlined; fragments that moved are marked with an X (Sept. 12, 1967).

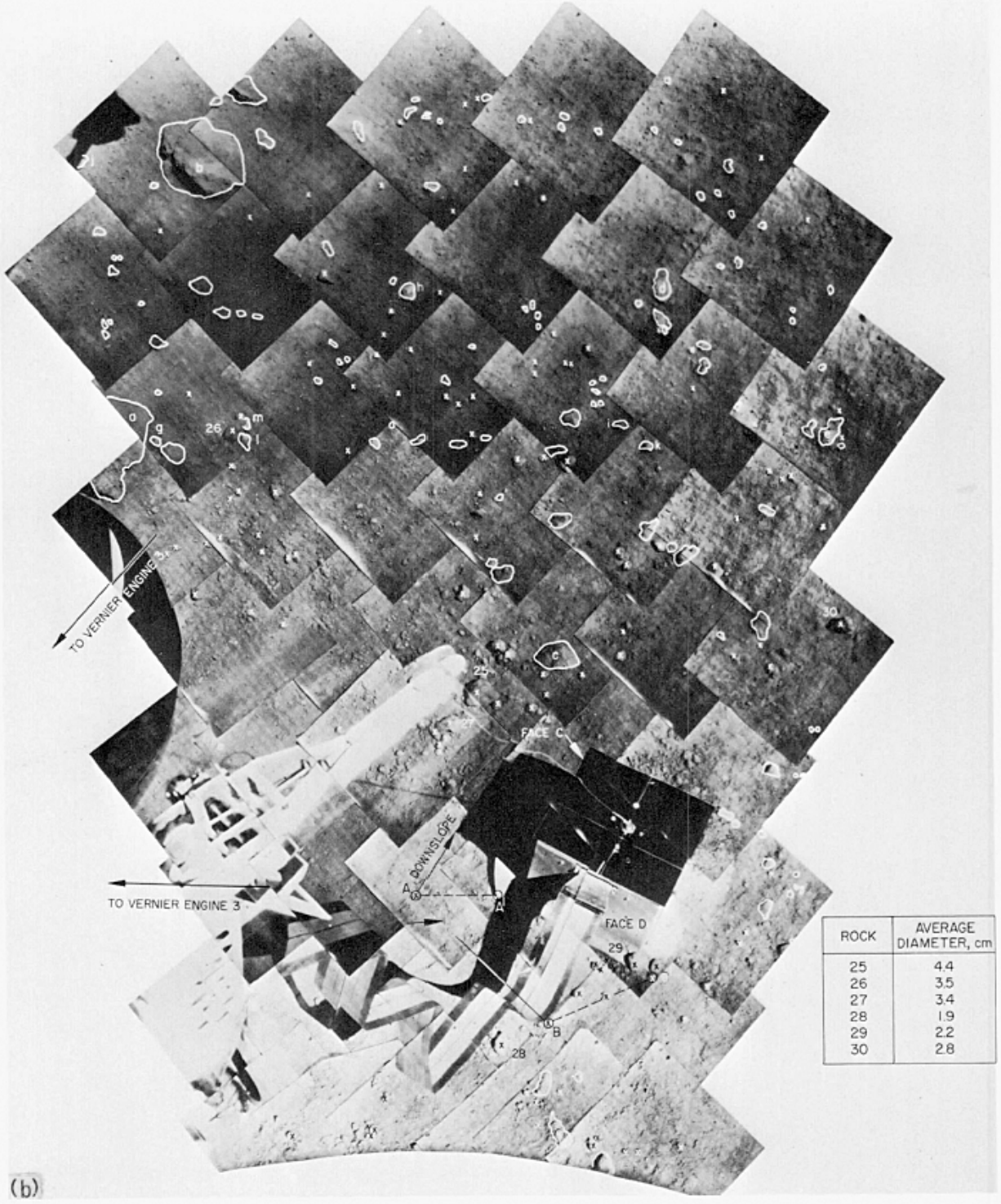

ROCK	AVERAGE DIAMETER, cm
25	4.4
26	3.5
27	3.4
28	1.9
29	2.2
30	2.8

FIGURE 4–18.—Concluded.

figure 4–22, include: (1) fine, dark soil deposited in rays by engine 2 at *A*, *B*, and *C;* (2) the partial filling of the shallow depression at *E;* (3) the large number of coarse soil fragments deposited by engine 2 at *D;* (4) the surface with a rippled appearance at I caused by differential erosion by engine 3; and (5) the fan of fine, dark soil deposited in rays at *M* by engine 1. One or more of the soil clumps ejected by the firing hit the photo-

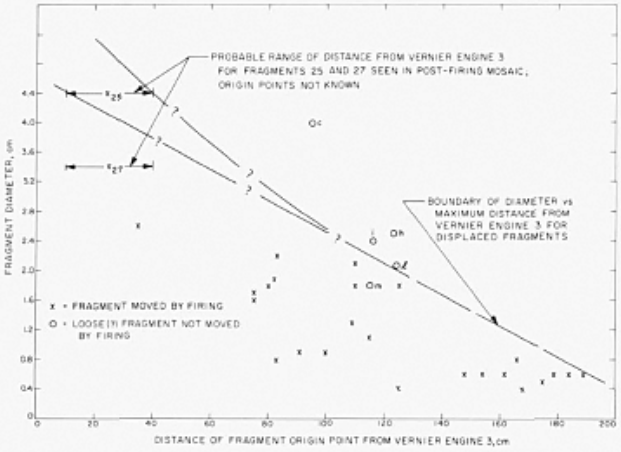

FIGURE 4–19.—Graph of diameter versus distance for fragments moved by the Surveyor V vernier engine 3 static firing. The dashed line represents the probable maximum sizes for fragments that could be moved by the firing at distances ranging from 10 to 200 cm.

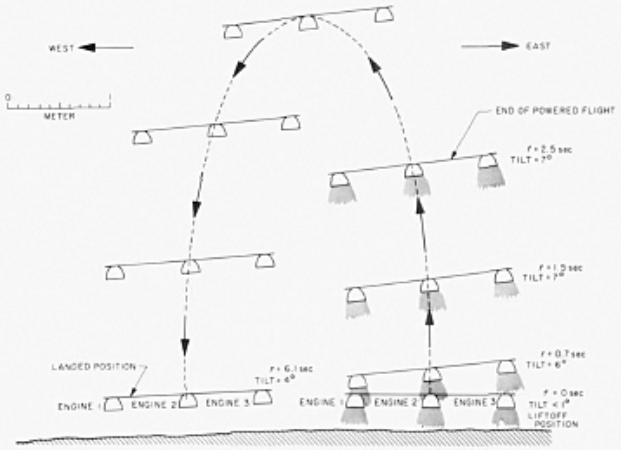

FIGURE 4–20.—Time sequence of vernier-engine positions during liftoff for the hop during the Surveyor VI mission. View is perpendicular to direction of hop.

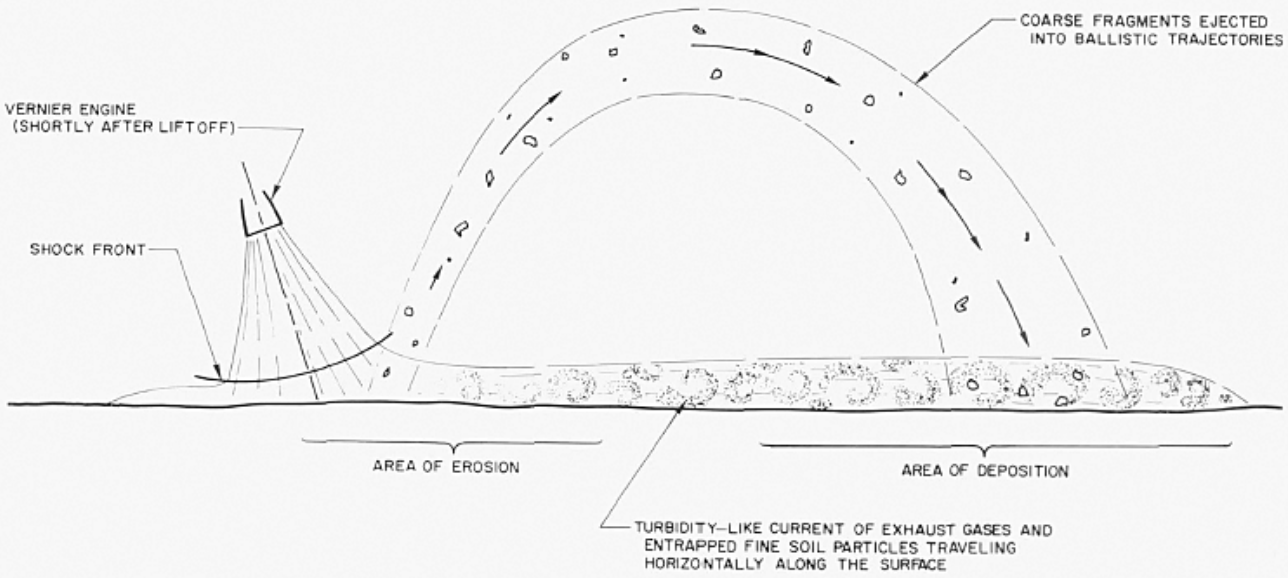

FIGURE 4–21.—Probable history of erosion in Surveyor VI vernier engine 2 area during hop.

metric target on one of the omnidirectional antennas and left a thick coating of soil adhering to the target (fig. 4–26).

Simulations and analyses.—The vernier-engine firing data and surface-pressure data for Surveyors III, V, and VI are summarized in table 4–3. The thrust levels listed were obtained from analytical simulations (Surveyors III and VI) and from strain gages on the vernier-engine support structure (Surveyor V). The minimum nozzle height listed for Surveyor III was estimated from the analytical simulations; those for Surveyors V and VI were obtained from comparisons of Surveyor pictures and photographs of laboratory simulations using a full-scale spacecraft (refs. 4–3 and 4–4). The lunar surface areas in the vicinity of Surveyor III engines 1 and 2 could not be viewed directly; therefore, their minimum nozzle heights are not included.

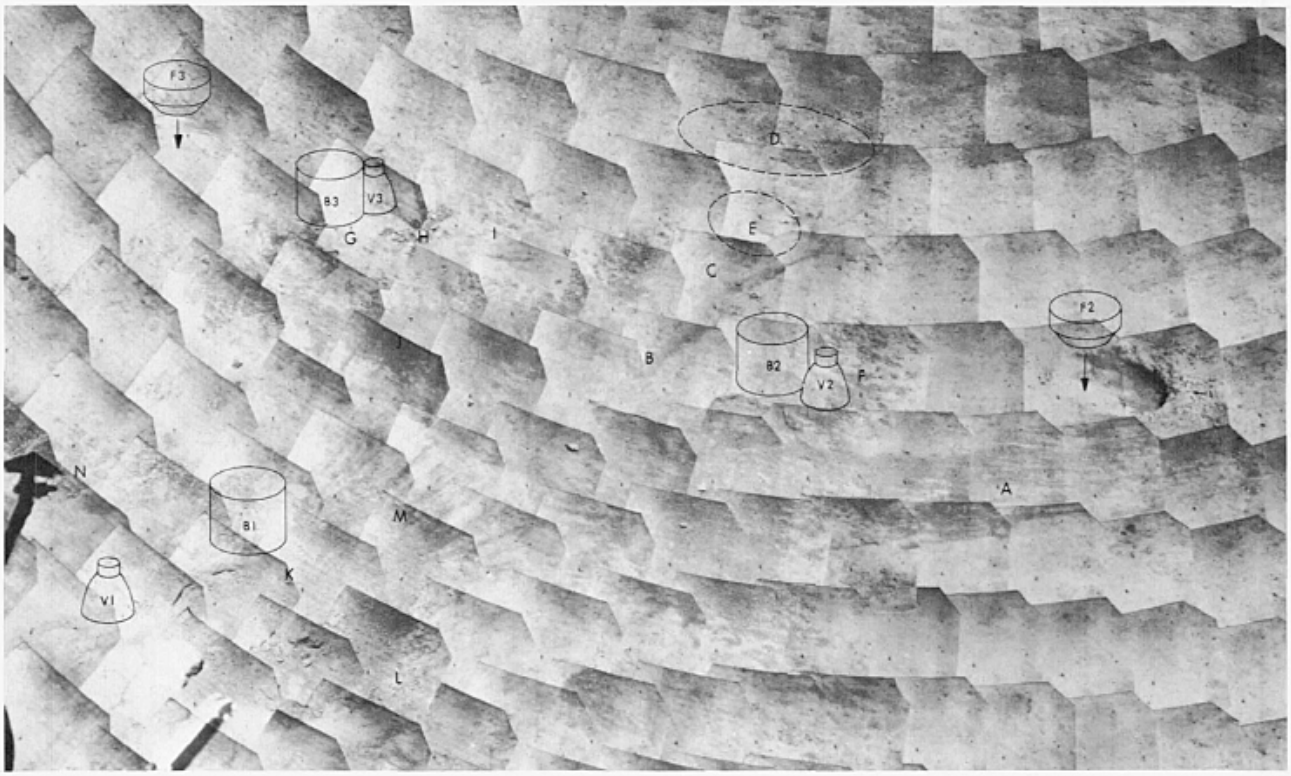

FIGURE 4–22.—Mosaic of posthop, computer-processed pictures showing the (1) approximate locations of the crushable blocks and vernier engines before liftoff for the hop; (2) the images of footpads above their final imprints made during the original landing; and the principal areas of erosion caused by the vernier engines during liftoff for the hop as indicated by capital letters (Nov. 15 and 16, 1967, Catalog 6–SE–22).

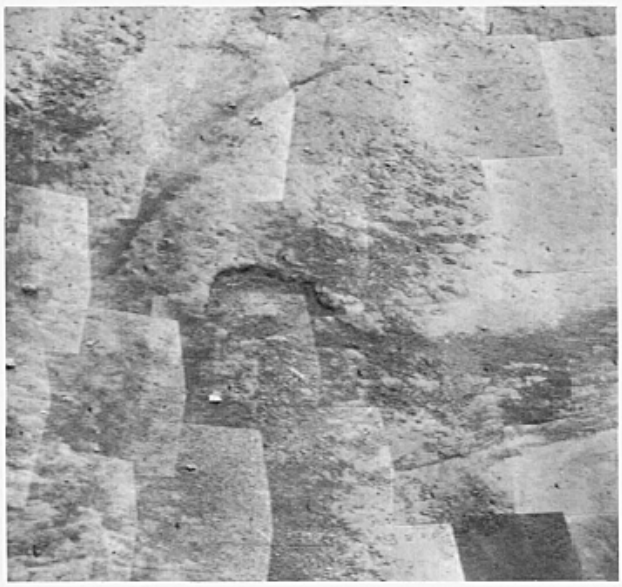

FIGURE 4–23.—Mosaic of computer-processed pictures, showing rays of fine, dark soil deposited by Surveyor V vernier engine 2 during the hop (Nov. 15 and 16, 1967, Catalog 6–SE–43C).

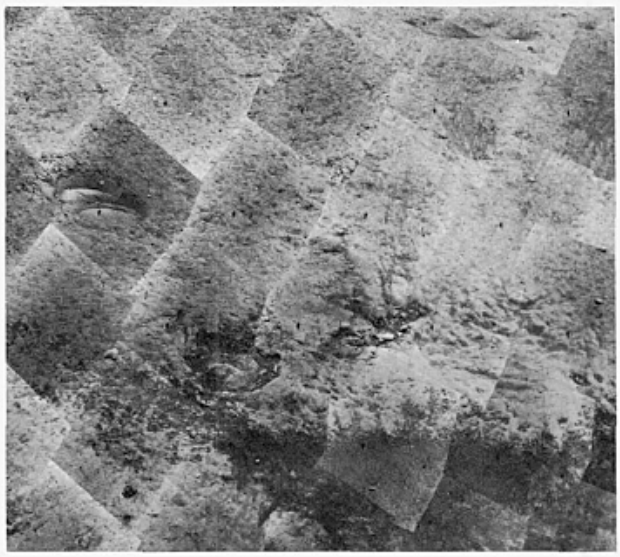

FIGURE 4–24.—Mosaic of computer-processed pictures, showing imprints of footpad 3 and crushable block 3 made during the initial landing and soil disturbance caused by Surveyor VI vernier engine 3 during the hop (Nov. 15 and 16, 1967, Catalog 6–SE–43B).

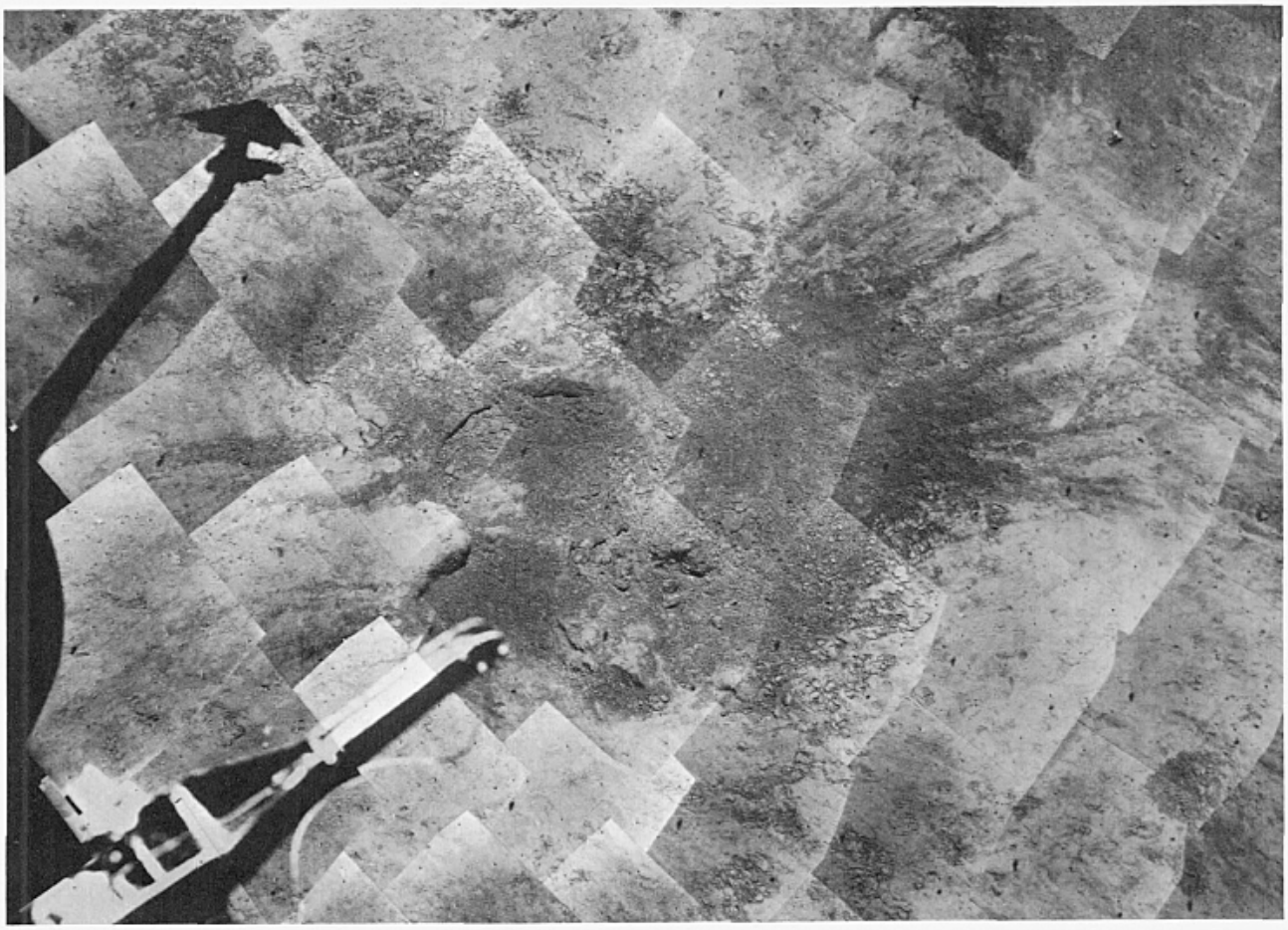

FIGURE 4–25.—Mosaic of computer-processed pictures, showing crushable block 1 impact area and soil disturbance caused by Surveyor VI vernier engine 1 during the hop (Nov. 15 and 16, 1967, Catalog 6–SE–43A).

TABLE 4-3. *Vernier-engine parameters used in computations*

Parameter	Surveyor III			Surveyor V			Surveyor VI		
	Engine 1	Engine 2	Engine 3	Engine 1	Engine 2	Engine 3	Engine 1	Engine 2	Engine 3
Maximum thrust, N	490	130	250	120	76	120	390	310	420
Nozzle exit plane height,[a] cm	------	------	25	39	39	39	32	32	32
Maximum static pressure, N/cm²	------	------	0. 50	0. 29	0. 18	0. 29	0. 69	0. 92	1. 35
Maximum dynamic pressure, N/cm²	------	------	0. 22	0. 12	0. 076	0. 12	0. 30	0. 39	0. 56

[a] Tabulated values correspond to the minimum nozzle heights used in the surface loading computations. Although some of these values were subsequently revised, the tabulated surface pressures still provide representative estimates.

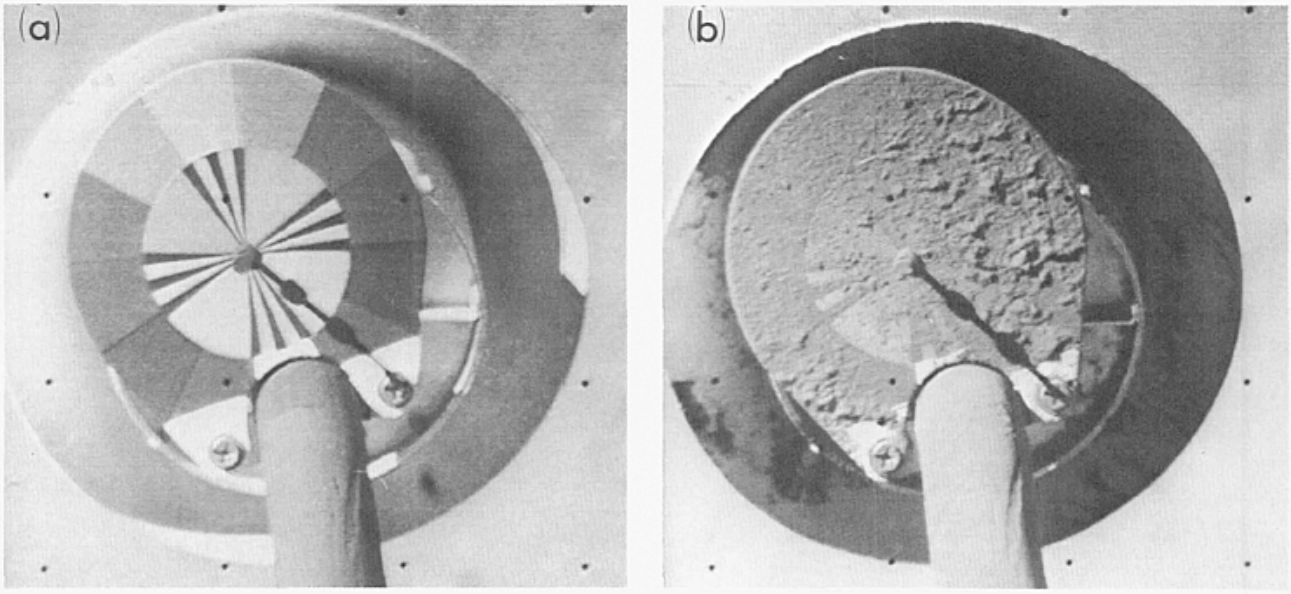

FIGURE 4–26.—Surveyor VI photometric target on omnidirectional antenna boom. (a) Prefiring picture (Nov. 15, 1967, 09:37:11 GMT). (b) Postfiring picture. Before the firing, the target was clean; after the firing, the target was coated with a layer of soil up to 0.9 mm thick. The coating probably was caused by impact of a soil clump on the target during the firing (Nov. 15, 1967, 12:30:00 GMT).

The maximum static and dynamic surface pressures listed in table 4–3 are values obtained from Roberts' theory (refs. 4–14 and 4–15). Figure 4–27 shows the relationship between these pressures and gas velocity versus radial distance. The dynamic pressure is equal to $\rho u^2/2$, where ρ is the gas mass density and u the radial velocity of the gas along the surface. The values for the Surveyor V static firing correspond to the engine thrusts and nozzle heights given in table 4–3. The pressures given for Surveyors III and VI are the maximum values encountered during the second Surveyor III landing event and Surveyor VI hop, respectively. During these maneuvers, maximum engine thrusts and minimum nozzle heights did not occur simultaneously; therefore, the lifted maximum surface pressures did not correspond to both maximum thrusts and minimum nozzle heights.

The viscous erosion theory given in references 4–14 and 4–15 was used to compare the theoretical and observed crater dimensions. Theoretically, soils composed of particle sizes smaller than 500 microns would not erode as fast as observed during the Surveyor V firing. Also, for a hypothetical soil composed of 600-micron particles and with a cohesion of 0.01 N/cm^2 (selected to approximate the average erosion rate), the theoretical erosion crater diameter would be 70 cm instead of the measured 20-cm-diameter crater under the Surveyor V vernier engine 3. These calculations indicate that viscous erosion was not the major erosion mechanism for the formation of the crater. However, viscous erosion probably caused the larger soil fragments to move across the surface from positions outside the crater.

Since viscous erosion does not appear to have been the principal eroding mechanism, it is thought that diffused gas eruption occurred. This type of erosion, however, does not provide an estimate on cohesion of the surface material because the diameter of a diffused gas eruption crater is largely independent of the soil cohesion (ref. 4–17). But it can be concluded, by comparing the calculated crater diameter with the observed value, that the lunar soil must be relatively impermeable; a firing time of 0.5 second (Surveyor V) is only one-tenth of the time required to reach steady-state conditions. This is based on an assumed soil porosity between 0.3 and 0.5 and a viscosity of the exhaust gases in the soil between 1×10^{-4} and

3×10^{-4} poise, as explained in reference 4–17. From this, the permeability of the soil was calculated to be between 1×10^{-8} and 7×10^{-8} cm^2.

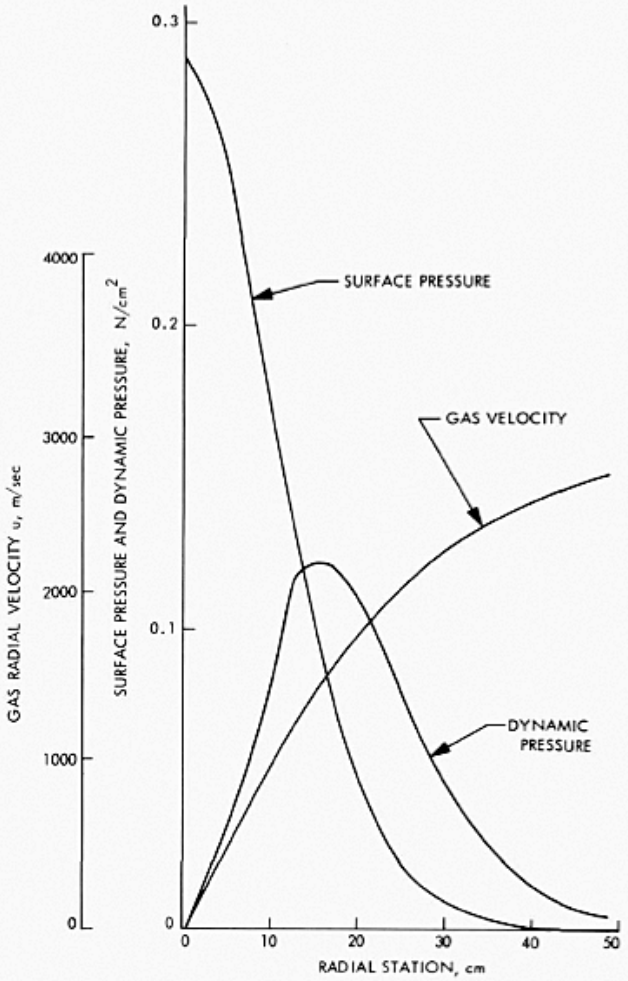

FIGURE 4–27.—Theoretical static pressure, dynamic pressure, and exhaust gas radial velocity at the surface of a plane, parallel to the engine nozzle exit plane; engine thrust=120 N, nozzle exit plane height=39.4 cm.

For comparison, the permeabilities of soils of different uniform grain sizes are shown in figure 4–28. This figure shows that the permeability range for the lunar surface material, probably down to a depth of about 25 cm, fits into the permeability range of silts (grain-size range from 2 to 60 microns). Lunar soil contains particles larger, and probably smaller, than this range. However, the estimated lunar permeability indicates that most of the particles are in the 2- to 60-micron size range. This estimate is in agreement with conclusions reached from light reflectance simulations of Surveyor III footpad imprints (ref. 4–2).

Estimates of soil cohesion.—Results of the Surveyor VI erosion test were used to estimate bounds for the cohesion of the lunar soil. Pictures of the Surveyor VI landing site (fig. 4–22) indicate some surface erosion, apparently of the viscous type, occurred beneath and adjacent to each engine during liftoff. There is no indication that bearing load cratering occurred. During takeoff for the Surveyor VI hop, the exhaust gas pressure on the lunar surface decreased gradually enough to prevent diffused gas eruption of the soil. Therefore, the estimates for soil cohesion are based on the conclusion that the cohesion was not large enough to prevent viscous erosion, but large enough for the soil to withstand vertical pressure loading.

According to the theory advanced in references 4–14 and 4–15, the maximum erosive shear stress occurs at the point of maximum dynamic pressure and is dependent on the effective value of the friction coefficient. Soil erosion data obtained by the Langley Research Center from soils having an initial flat surface indicated the effective friction coefficient, C_f, to be

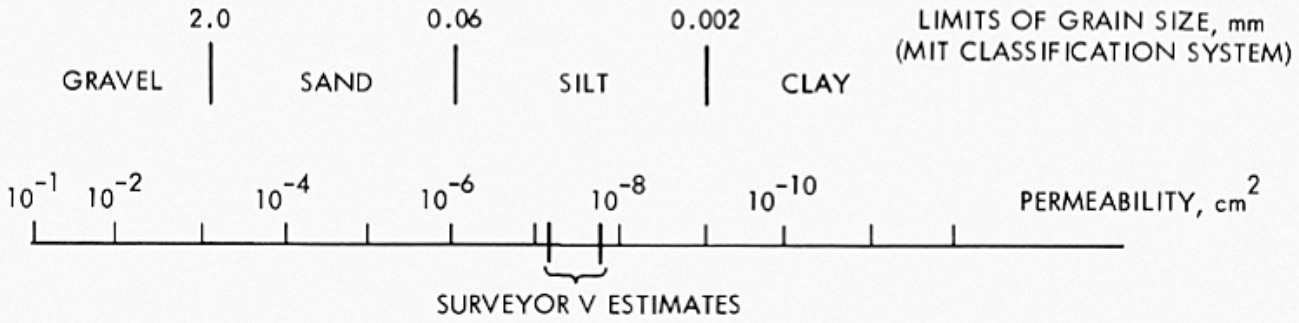

FIGURE 4–28.—Permeability of terrestrial soils versus grain size and classification related to Surveyor V results.

about 0.2, which is the value recommended in reference 4–15. For the irregular, undulating surface existing at the Surveyor VI landing site, the friction coefficient should be higher than 0.2. For the upper-bound estimate made here, C_f is taken as 0.4. According to table 4–3, the peak dynamic pressures under vernier engines 1, 2, and 3 were 0.30, 0.39, and 0.56 N/cm^2, respectively. Thus, for a friction coefficient of 0.4, the lunar surface was subjected to maximum shearing stresses of 0.12, 0.16, and 0.23 N/cm^2 by exhaust gases from vernier engines 1, 2, and 3, respectively.

Also, according to the theory in references 4–14 and 4–15, the viscous shear stresses are resisted by the frictional and cohesional forces of the soil. The resistance of the soil surface provided by the friction forces between soil grains is negligible for the small-diameter particles at the Surveyor VI landing site. As a result, erosion is essentially resisted by cohesion; therefore, upper-bound estimates of soil cohesion are equal to the maximum values of applied shearing stresses. Because each vernier engine caused some soil erosion, the minimum value for an upper-bound soil cohesion estimate is the shear stress caused by vernier engine 1. This value is 0.12 N/cm^2.

The maximum surface loading (1.35 N/cm^2) occurred under vernier engine 3. Under the assumption that Terzaghi's bearing-capacity theory (ref. 4–19) is applicable for this type of surface loading, estimates can be made for the minimum value of soil cohesion needed to prevent a bearing-capacity failure for various values of soil density and internal friction angle. An application of this theory, in conjunction with the pressure loading from Roberts' theory, indicates that a soil with an assumed weight density of 2.4×10^{-3} N/cm^3 (1.5-g/cm^3 mass density) and a soil cohesion greater than 0.0073 N/cm^2 would be sufficient to prevent a bearing-capacity failure for a soil with a 35° internal friction angle. For a friction angle of 30°, the required value of cohesion is 0.020 N/cm^2. Since a bearing capacity type of failure was not observed during the hop, this procedure indicates that the soil cohesion lower bound is 0.0073 N/cm^2.

Attitude Control Jet Operations

Observations.—Attitude control gas jets mounted on all Surveyor legs provided attitude stabilization during the flights. After landing, Surveyor I attitude control jets were operated to produce short pulses of 20-msec durations with a 30-msec pause between pulses (ref. 4–1). Pictures taken after operation of the jets revealed the presence of a small dimple crater near the attitude control jet 2 area of impingement. However, results of this test are inconclusive because no suitable prefiring pictures of the impingement area are available.

The attitude control jets on Surveyor VI were commanded to operate for a continuous burst of 4 seconds and for another burst of 60 seconds (ref. 4–4). Good television coverage of the jet impingement area on the lunar surface before, during, and after jet operation afforded clear observations of the surface erosion caused by attitude control jet 2. The nozzle of this jet was about 10.4 cm above the surface and was inclined 24° from the spacecraft vertical axis.

Comparisons of pictures taken before and after each burst (fig. 4–29) show that the disturbance of the lunar surface caused by the jet operations was minor and that no crater was formed. Some small soil fragments up to 25 cm from the impingement area were moved by the jet operation. The most conspicuous effect consisted of the movement of two lunar surface protrusions, probably soil clumps, which were 12 to 15 cm from the center of jet impingement (fragments *A* and *B*, fig. 4–29).

Simulations and analyses.—Laboratory tests were performed in which an attitude control jet was operated over soil beds in vacuum. The soil erosion caused by the jet was of the viscous type; no eruption caused by diffused gas was observed.

It was found that erosion occurred if the soil cohesion was below a limiting value. For the sandy silts used in these tests, the limiting value of the cohesion was 0.17 N/cm^2. However, these tests were conducted at a pressure of approximately 50×10^{-3} mm Hg and full expansion of the jet plume probably did not occur. Therefore, static pressure on the soil surface in the vacuum chamber probably was greater than on the lunar surface beneath the jet.

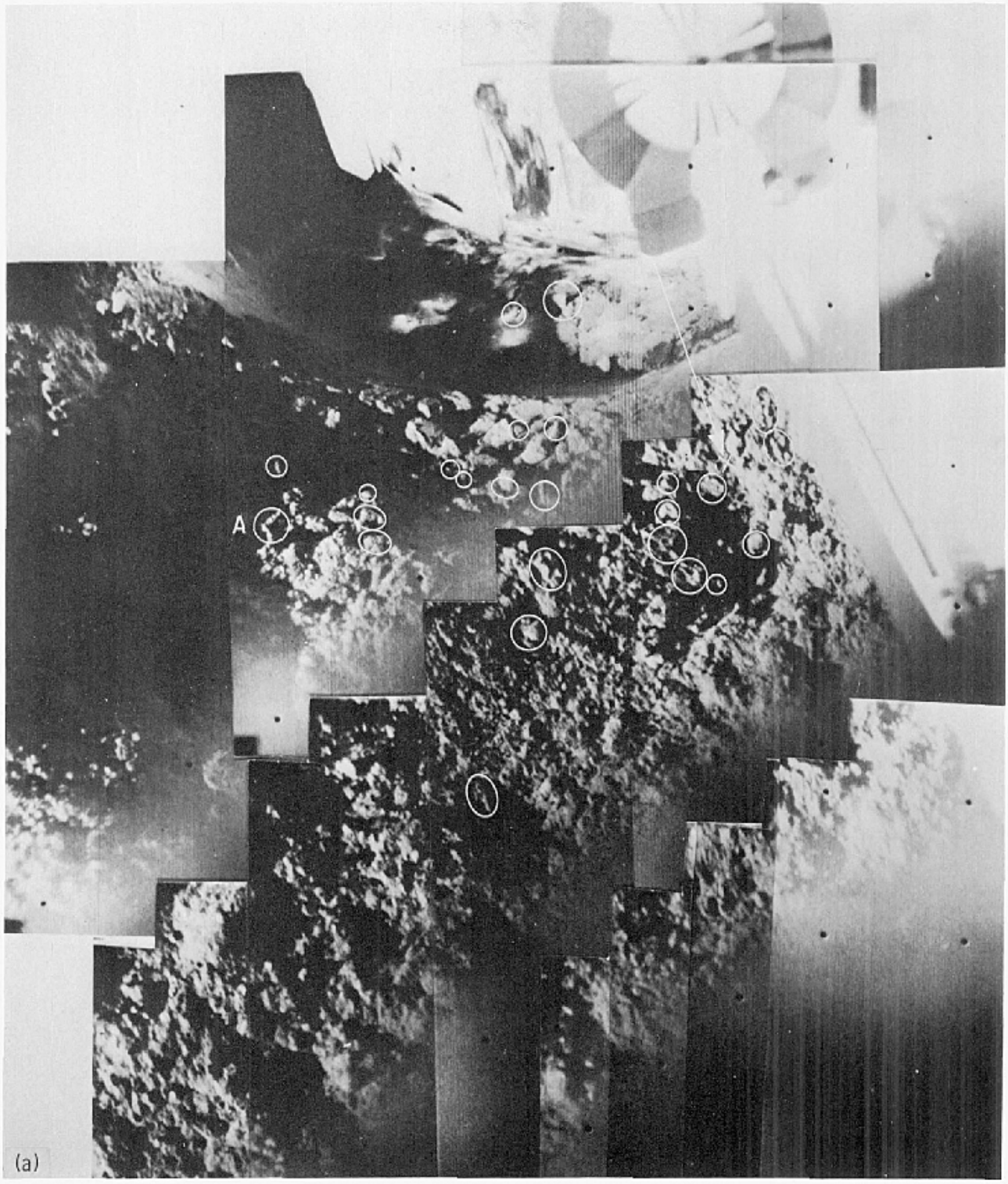

FIGURE 4–29.—(a) Mosaic of narrow-angle pictures taken shortly before the 4-second operation of the attitude control jets. Representative fragments, shown by postoperation pictures to have moved or to have been partially eroded by the firing, are circled. The dark area cutting diagonally across each picture is the camera housing. A line extending through the center of the attitude control jet is shown by the arrow. The approximate point where this line intercepts the lunar surface is shown by an X (Nov. 9, 1967, Catalog 6–MP–1).

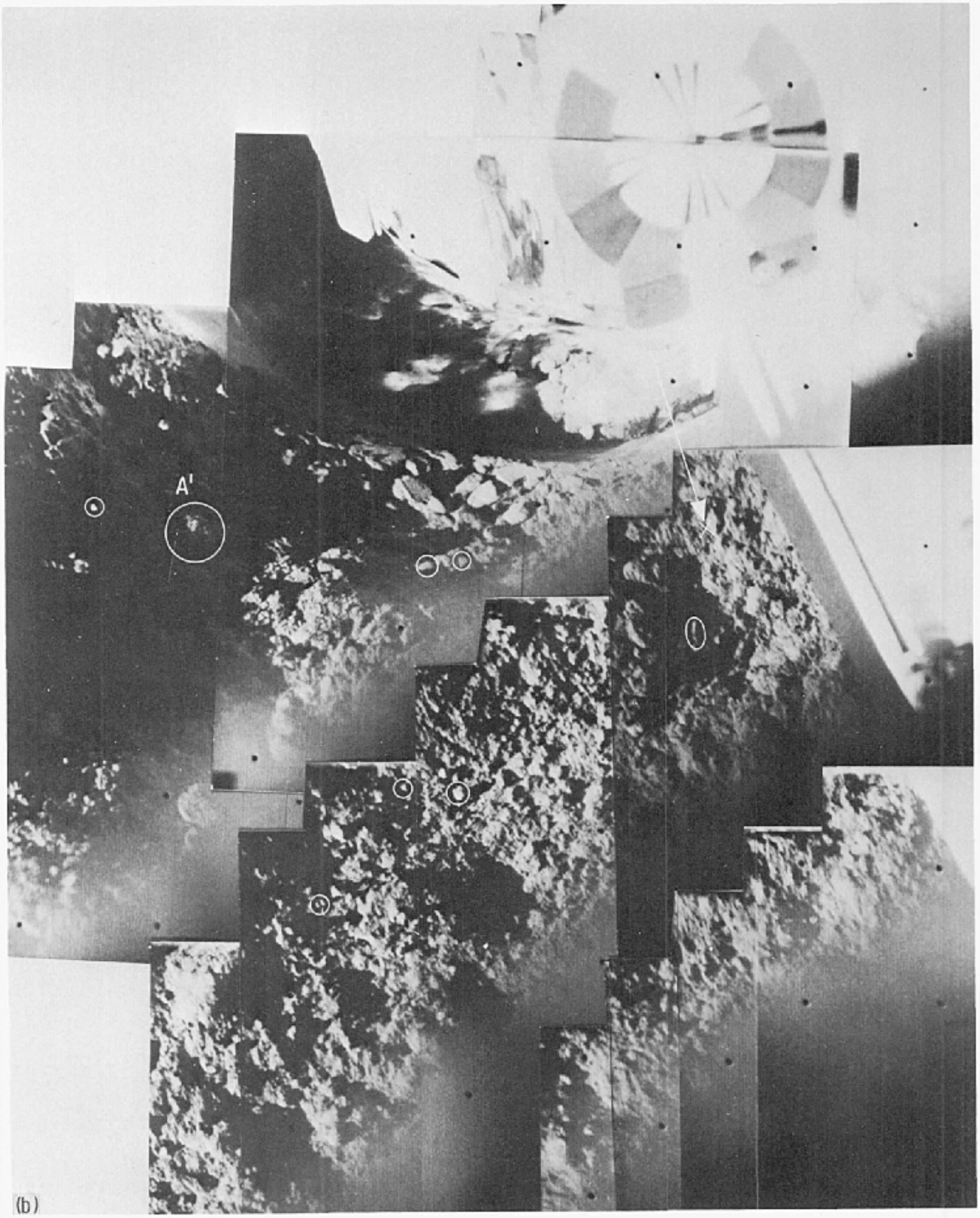

FIGURE 4–29.—Continued. (b) Mosaic of pictures taken immediately after the 4-second firing of the attitude control jets. Representative fragments that arrived at their present sites because of the firing are circled (Nov. 9, 1967, Catalog 6–MP–2).

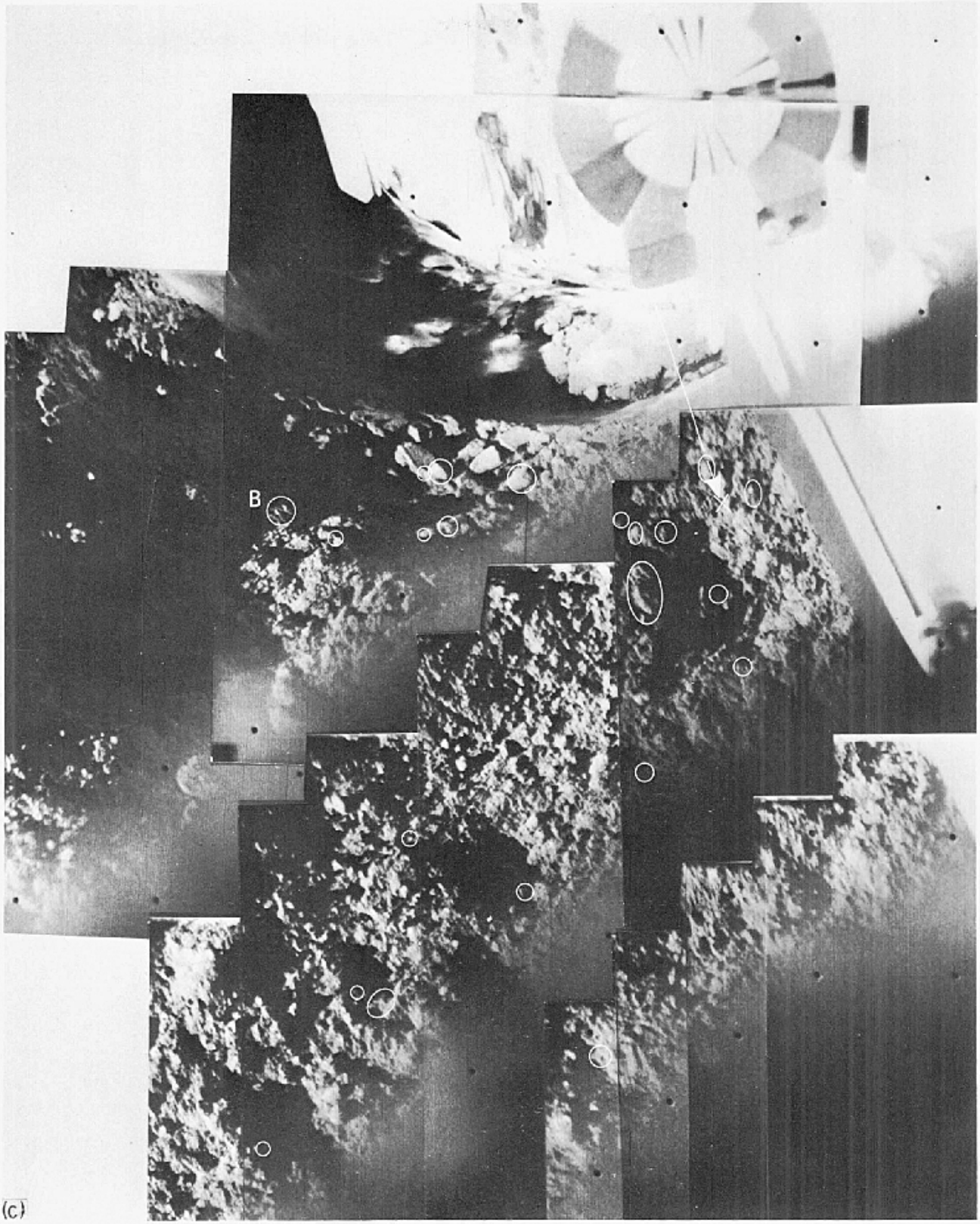

FIGURE 4–29.—Continued. (c) Mosaic of the same pictures used in figure 4–29(b); however, the fragments circled are those fragments shown by later pictures to have been moved by the 60-second attitude control jet firing (Nov. 9, 1967, Catalog 6–MP–2).

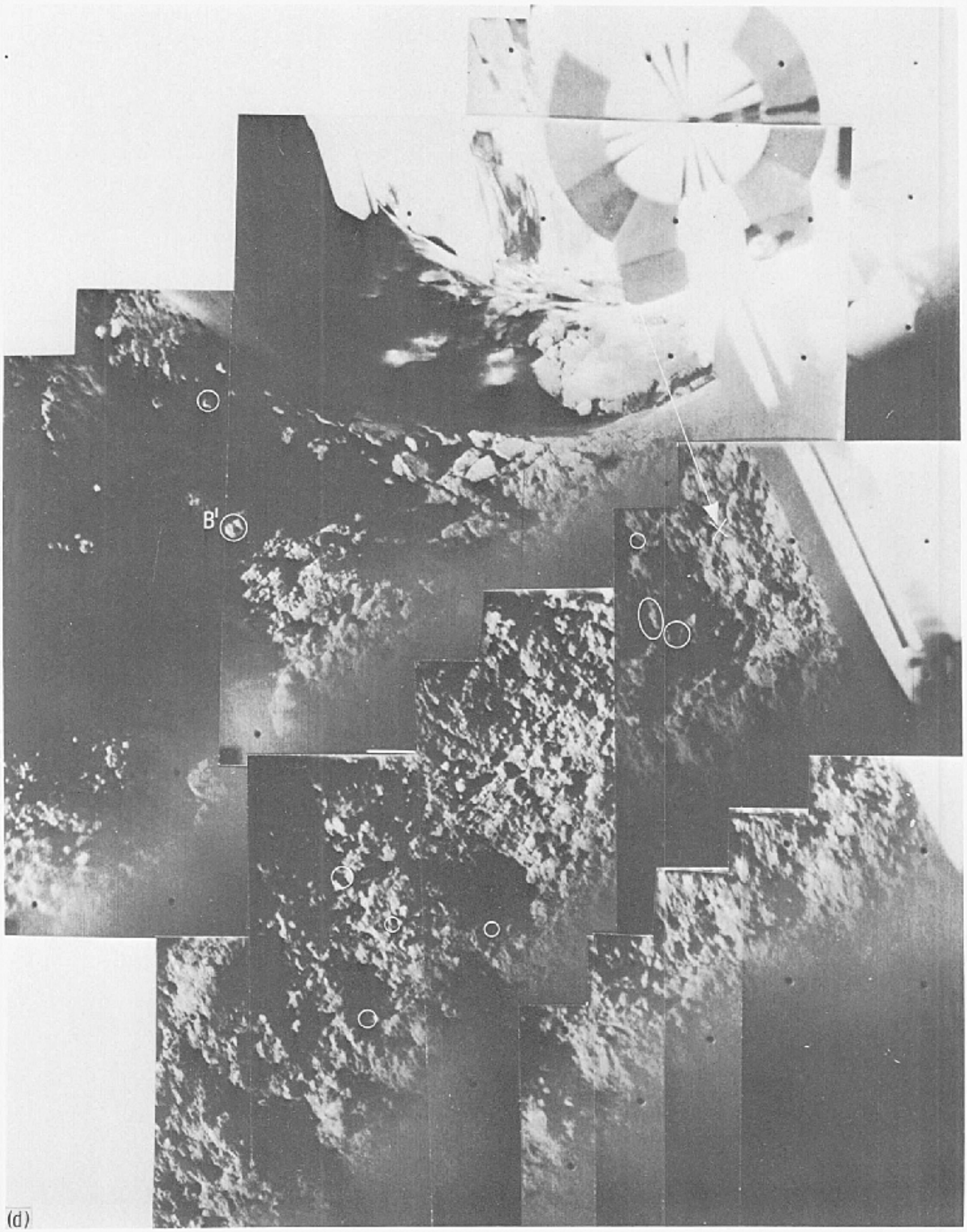

FIGURE 4–29.—Concluded. (d) Mosaic of pictures taken after the 60-second attitude control jet firing. Fragments circled arrived at their present sites after the 60-second firing (Nov. 9, 1967, Catalog 6–MP–3).